第 28 卷第 12 期 无 机 化 学 学 报 Vol.28 No.12
2012 年 12 月 CHINESE JOURNAL OF INORGANIC CHEMISTRY 2597-2604

镧含量对 La-$SrTiO_3$ 催化剂的结构和光催化活性的影响

李慧泉[1,2] 崔玉民*[,1,2] 吴兴才*[,3] 洪文珊[1] 华 林[4]
([1]阜阳师范学院化学化工学院,阜阳 236041)
([2]安徽环境污染物降解与监测省级实验室,阜阳 236041)
([3]南京大学化学系介观化学教育部重点实验室,配位化学国家重点实验室,南京 210093)
([4]R&D 研发中心,新加坡 059818)

摘要: 采用溶胶–凝胶方法制备了不同 La 含量掺杂 $SrTiO_3$ 催化剂,通过 X 射线光电子能谱(XPS)、X 射线衍射(XRD)、扫描电子显微镜(SEM)、透射电子显微镜(TEM)、紫外–可见漫反射光谱(UV-Vis DRS)和 BET 比表面积测量对其进行了表征,用甲基橙(MO)催化降解实验评价了其光催化活性。结果表明:钛酸锶经镧掺杂后仍然保持了钙钛矿结构;与纯 $SrTiO_3$ 相比,0.5% La-$SrTiO_3$ 样品的粒子大小和形貌没有大的区别,但它的吸收带边发生明显红移;La-$SrTiO_3$ 样品的紫外和可见光催化活性随 La 含量增加先增加,当 La 含量为 0.5%时分别达到最大值,然后随 La 含量的进一步增加而减小;与纯 $SrTiO_3$ 相比,0.5% La-$SrTiO_3$ 样品明显具有更高的紫外和可见光催化活性,这改善的光催化活性主要归因于比表面积增加、吸附性能提高、在 250~650 nm 区域有较强的光吸收和较低的禁带能级。

关键词: 溶胶–凝胶法; 镧掺杂; 钛酸锶; 光催化
中图分类号: O634 **文献标识码**: A **文章编号**: 1001-4861(2012)12-2597-08

Effect of La Contents on the Structure and Photocatalytic Activity of La-$SrTiO_3$ Catalysts

LI Hui-Quan[1,2] CUI Yu-Min[1,2] WU Xing-Cai*[,3] HONG Wen-Shan[1] HUA Lin[4]
([1]*School of Chemistry and Chemical Engineering, Fuyang Normal College, Fuyang, Anhui* 236041, *China*)
([2]*Anhui Provincial Key Laboratory for Degradation and Monitoring of Pollution of the Environment, Fuyang, Anhui* 236041, *China*)
([3]*Key Laboratory of Mesoscopic Chemistry of MOE, The State Key Laboratory of Coordination Chemistry, School of Chemistry and Chemical Engineering, Nanjing University, Nanjing* 210093, *China*)
([4]*R&D Center, Singapore Linovus Technology Pte Ltd*, 059818, *Singapore*)

Abstract: La-doped $SrTiO_3$ catalysts with different La contents were prepared by a sol-gel method, and characterized by X-ray photoelectron spectroscopy (XPS), X-ray diffraction (XRD), scanning electron microscopy (SEM), transmission electron microscopy (TEM), UV-Vis diffuse reflectance spectra (UV-Vis DRS), and low temperature nitrogen adsorption. The photocatalytic activities were evaluated by photo-degradation of methyl orange (MO). The results show that La-doped $SrTiO_3$ keeps a perovskite structure and the absorption edge of 0.5% La-$SrTiO_3$ sample is obviously red-shifted. There is no big difference between pure $SrTiO_3$ and 0.5% La-$SrTiO_3$ samples in particle size and morphologies. With the increase of La content, the photocatalytic activities of La-$SrTiO_3$ samples under UV and visible light irradiation first increase, reaching a maximums around La content of 0.5%, and then decrease with further increasing La. Compared with pure $SrTiO_3$, the 0.5% La-$SrTiO_3$ sample obviously exhibits much higher UV and visible light photocatalytic activity. The enhanced photocatalytic activity can be mainly attributed to the increase of BET surface area, the enhancement in adsorption performance, the stronger absorption in 250~650 nm light region and the lower band-gap energy level.

Key words: sol-gel method; La-doped; $SrTiO_3$; photocatalysis

收稿日期:2012-04-15。收修改稿日期:2012-05-29。
国家自然科学基金(No.21171091),安徽省高校省级自然科学研究课题(KJ2012A217,KJ2012B136)资助项目。
*通讯联系人。E-mail:cymlh@fync.edu.cn,(FAX):+86 558 2596 703,wuxingca@nju.edu.cn,FAX:+86 25 8331 7761

As one of the most promising photocatalysts, $SrTiO_3$ has been widely researched for the photocatalytic degradation of organic pollutants in the past decades [1-4]. However, the intrinsic property of $SrTiO_3$ (wide band-gap energy level, ~3.2 eV) limits its applications in solar light containing less than 5% of ultraviolet light (λ <400 nm). Therefore, to extend its activity into the visible light region, many attempts have been devoted to doping of transition metal ions and non-metal elements into $SrTiO_3$ [5-8]. For example, the Fe-doped $SrTiO_3$ has been shown to have a much higher photocatalytic activity than pure $SrTiO_3$ for the degradation of RhB under visible light irradiation [5]. Recently, noble metals such as Ag, Pt and Au have been reported as dopants of $SrTiO_3$ to enhance the visible light response [4]. La^{3+} has nearly the same ionic radius (115 pm) as Sr^{2+} (113 pm) and the Sr^{2+} ions in $SrTiO_3$ can be isomorphic substituted by La^{3+} ions without producing a large lattice strain. However, to the best of our knowledge, there has been no report on the study of the structure and photocatalytic activity for $SrTiO_3$ doped with La.

The aim of the present work is to synthesize La-doped $SrTiO_3$ catalysts with different La contents by a sol-gel method and to investigate the effect of La on the structure and photocatalytic activity of La-$SrTiO_3$ samples.

1 Experimental

1.1 Catalyst preparation

A typical synthesis procedure of La-doped $SrTiO_3$ was carried out as follows: 5.0 mL of tetrabutyl titanate, 8.5 mL of acetic acid glacial and 8.0 mL of deionized water were mixed under continuous stirring until a clear solution was obtained. Then, 5.0 mL of deionized water with a stoichiometry of strontium chloride hexahydrate, and a certain amount of La precursors was added dropwise. Finally, 12 mL of 4.0 mol·L^{-1} citric acid solution was added to adjust the pH value to about 1.50. The resulting solution was stirred for 0.5 h at room temperature, then heated to 338 K by water bath and kept at this temperature for 4.0 h in a closed system. Most of the water was evaporated slowly at this temperature in another 5.0 h and the solution turned very viscous. After that, the solution was dried thoroughly at 383 K for 10 h and at 453 K for another 10 h. The brown powder was obtained after milling. The catalysts of La-doped $SrTiO_3$ were produced by calcining the powder at 673 K for 10 h and then at 923 K for another 10 h in air. For comparison, the pure $SrTiO_3$ was prepared using the same method. The final samples with original La/$SrTiO_3$ molar ratios of 0.000, 0.002, 0.005, 0.010, and 0.020 were denoted as 0.0%, 0.2%, 0.5%, 1.0% and 2.0% La-$SrTiO_3$, respectively.

1.2 Catalyst characterization

X-ray diffraction were performed on a Philips X′ pert diffractometer equipped with Ni-filtered Cu $K\alpha$ radiation source (λ=0.15418 nm). The X-ray tube was operated at 40 kV and 40 mA. X-ray photoelectron spectroscopy (XPS) measurements were carried out using Multilab 2000 XPS system with a monochromatic Mg $K\alpha$ source and a charge neutralizer. All binding energies were referenced to contaminant carbon (C1*s*= 284.6 eV). Scanning electron microscopy (SEM) images were recorded on an X-650 microscope operated at 25.0 kV. Microstructures were observed by a transmission electron micrograph (TEM, JEOL JEM-2010). The BET surface areas of samples were determined from N_2 adsorption isotherms at −196 ℃ using a Micromeritics ASAP 2020 instrument with a computer-controlled measurement system. Prior to analysis, 0.05 ~0.15 g catalyst samples were degassed at 250 ℃ and 10 mmHg. UV-Vis diffuse reflectance spectra (UV-Vis DRS) of the catalysts were determined with a Shimadzu UV-3600 spectrophotometer using $BaSO_4$ as a reference. The actual La/$SrTiO_3$ molar ratios of the obtained La-$SrTiO_3$ photocatalysts were detected by IRIS (INTREPID 2) inductively coupled plasma atomic emission spectrometry (ICP-AES, ICP710, Varian, America).

1.3 Photocatalytic activity

The photocatalytic activities of La-doped $SrTiO_3$ catalysts were evaluated by the degradation of methyl orange (MO) in an aqueous solution. The UV light was obtained by a 300 W high-pressure mercury lamp (λ_{max}= 365 nm). The visible light source was a 500 W Xenon-

arc lamp (λ_{max}=470 nm) with the combination of a cut-off filter (>400 nm) to eliminate UV radiation during visible light experiments. For each UV and visible light test, 40 mL MO aqueous solution (7.64×10^{-6} mol·L^{-1}) and 0.2 g catalyst was used. A general procedure was carried out as follows. First, MO aqueous solution was placed into a water-jacketed reactor maintained at 25 ℃, and then the catalyst samples were suspended in the solution. The suspension was stirred vigorously for 0.5 h in the dark to establish the adsorption-desorption equilibrium of MO, then irradiated under UV or visible light. About 3.0 mL solution was withdrawn from the reactor periodically and centrifuged and analyzed for the degradation of MO using a UV-2450 UV-Vis spectrophotometer. MO has a maximum absorbance at 464 nm, which was used as a value for monitoring MO degradation. The absorbance was converted to the MO concentration in accordance with a standard curve showing a linear relationship between the concentration and the absorbance at this wavelength.

2 Results and discussion

2.1 Catalyst structure

Fig.1 shows the XRD patterns of La-$SrTiO_3$ catalysts with different La contents. It can be seen that all samples exhibit special diffraction peaks of $SrTiO_3$, the peaks around 2θ of 22.7°, 32.2°, 39.8°, 46.4°, 52.1°, 57.7°, 67.8° and 77.1° are indexed to those of cubic perovskite structure of $SrTiO_3$ (PDF Card No. 35-734) and correspond to (100), (110), (111), (200), (210), (211), (220) and (310) respectively, and no other peaks were detected. The average crystalline sizes of $SrTiO_3$ (110) in the La-$SrTiO_3$ composites were calculated by the Scherrer formula and the results are listed in Table 1.

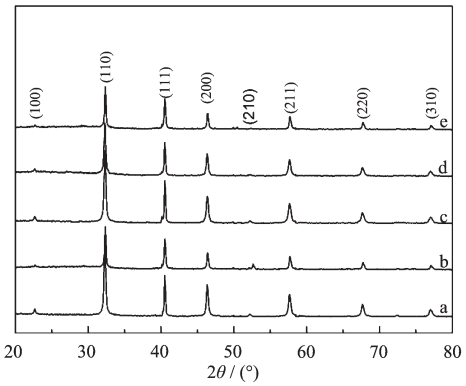

(a) 0.0; (b) 0.2; (c) 0.5; (d) 1.0; (e) 2.0

Fig.1 XRD patterns of La-$SrTiO_3$ catalysts with different La contents (mol %)

Table 1 XRD and BET results for different catalysts

Catalyst	Actual molar ratios / %	Average crystallite size / nm	BET surface area / (m^2·g^{-1})
$SrTiO_3$	0.00	28.7	16.4
0.2% La-$SrTiO_3$	0.19	26.1	19.7
0.5% La-$SrTiO_3$	0.47	25.8	22.3
1.0% La-$SrTiO_3$	0.95	25.3	24.1
2.0% La-$SrTiO_3$	1.93	25.6	23.2

The XPS spectra of $SrTiO_3$ and 0.5% La-$SrTiO_3$ are presented in Fig.2. No peaks attributed to La3*d* are found in region of 825~840 eV (La3*d*). It indicates that few of lanthanum atoms exists on the surface of 0.5% La-$SrTiO_3$ sample. The XPS spectra of Ti2*p* at around 457 eV and Sr3*d* at around 133 eV for the $SrTiO_3$ and 0.5% La-$SrTiO_3$ are shown in Fig.3 (A) and (B), respectively.

As shown in Fig.3, the binding energies of Ti2*p* does not give an obvious change after introduction of La into the lattice of $SrTiO_3$, indicating that the chemical environment around Ti atom is not strongly affected by doping. However, by careful comparison with $SrTiO_3$, it can be found that the binding energies of Ti2*p* and Sr3*d* shift slightly to lower values in 0.5% La-$SrTiO_3$ sample. On the basis of XRD and XPS results, it is reasonable to consider that La has been incorporated into the lattice of the $SrTiO_3$.

A and B of Fig.4 show the SEM morphologies of pure $SrTiO_3$ and 0.5% La-$SrTiO_3$ synthesized under the same condition, respectively. As seen in Fig.4, there is no big difference between two samples in particle size

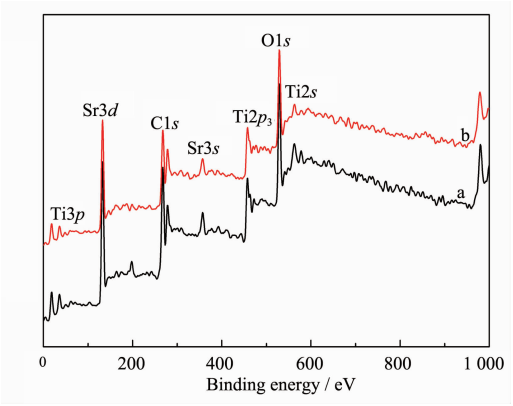

(a) $SrTiO_3$, (b) 0.5% La-$SrTiO_3$

Fig.2 X-ray photoelectron spectra of samples

($SrTiO_3$: ~68 nm; 0.5% La-$SrTiO_3$: ~60 nm) and morphologies. A careful observation finds that the particle in 0.5% La-$SrTiO_3$ looks a little bit smoother than that of pure $SrTiO_3$. It is reported that the particle with small size is favorable for the quick transportation of photogenerated carriers to the surface [9], whereas a rough surface might provide more effective reaction sites for photocatalysis [7]. Furthermore, the particle size and surface roughness differences between two samples are very little. Thus, the micro morphological differences of two samples should not be responsible for their different photocatalytic activities.

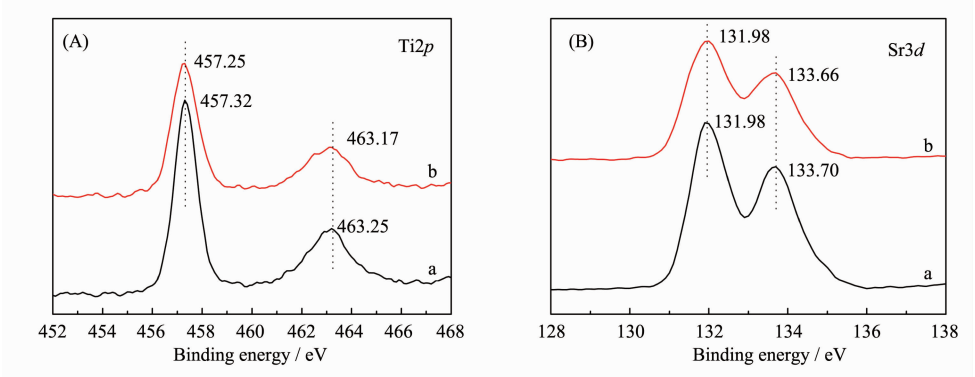

(a) $SrTiO_3$, (b) 0.5% La-$SrTiO_3$

Fig.3 XPS spectra of (A) Ti2*p* and (B) Sr3*d* for different samples

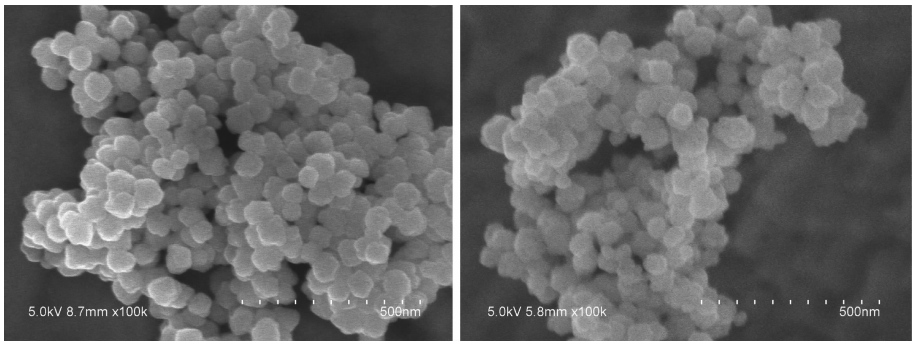

(A) $SrTiO_3$ (B) 0.5% La-$SrTiO_3$

Fig.4 SEM images of synthesized samples

Transmission electron microscopy (TEM) images for $SrTiO_3$ and 0.5% La-$SrTiO_3$ are shown in Fig.5. It exhibits a well-defined cubic morphology with an average particle size of about 70 nm for $SrTiO_3$ and a well-defined cubic morphology with an average particle size of 63 nm for 0.5% La-$SrTiO_3$, which confirms the nanostructure characteristic of for $SrTiO_3$ and 0.5% La-$SrTiO_3$. This result also shows that there is no big difference between two samples in particle size and morphologies. A careful observation also finds that the particle in 0.5% La-$SrTiO_3$ looks a little bit smoother than that of pure $SrTiO_3$, which is in agreement with the SEM results.

The BET surface areas of La-$SrTiO_3$ catalysts with

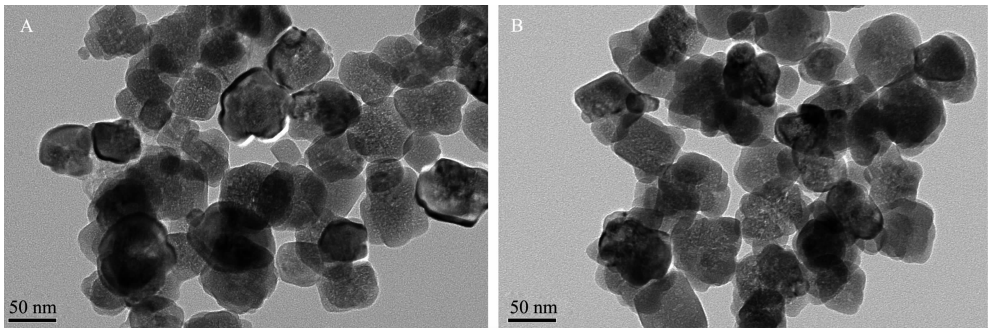

Fig.5　TEM images for (A) $SrTiO_3$ and (B) 0.5% La-$SrTiO_3$

different La contents are listed in Table 1. Obviously, incorporation of La into the $SrTiO_3$ inhibits the particle growth and thus increases its BET surface area. A large surface area can supply more active sites for the degradation reaction of organic compounds, resulting in a higher activity of the photocatalytic reaction.

2.2　Photocatalytic activity

The UV-Vis spectral of MO aqueous solution as a function of UV and visible light irradiation time in the presence of $SrTiO_3$ and 0.5% La-$SrTiO_3$ catalysts are illustrated in Fig.6 and Fig.7, respectively. It can be seen that the absorption peaks corresponding to MO diminish under UV and visible light irradiation indicate the degradation of MO and no new absorption bands are observed. It can be also seen that the visible region peak intensities in the photodegradation of MO by 0.5% La-$SrTiO_3$ catalyst decrease more obviously than that by pure $SrTiO_3$ catalyst during the same irradiation time, which is in agreement with the results of Fig.8. Photodegradation is rapid in the first 4.0 h and then slows down with the increase of irradiation time. This may be attributed to the gradual coverage of the active sites by the products of the reaction.

Fig.8 shows the UV and visible light photocatalytic activity of La-$SrTiO_3$ samples with different La contents. It can be seen that under UV and visible light irradiation the degradation of MO is much lower without photocatalyst in comparison, The $SrTiO_3$ and La-$SrTiO_3$ catalysts exhibit higher photocatalytic activities for MO degradation, and the La content in the $SrTiO_3$ exerts great influences on the photocatalytic activity of La-$SrTiO_3$ catalyst. With increasing La content, the photocatalytic activity of La-$SrTiO_3$ under UV and visible light irradiation first increases, reaching a maximum around La content of 0.5% and then decreases with further increasing La content. The 0.5% La-$SrTiO_3$ catalyst obviously exhibits much higher UV and visible light photoactivity than that of the Pure $SrTiO_3$ catalyst, indicating that doping of La in the $SrTiO_3$ with optimum La content remarkably enhances the photocatalytic activity of $SrTiO_3$.

To test the stability of the 0.5% La-$SrTiO_3$ catalyst for the photocatalytic reaction, the catalyst was reused for photocatalytic reaction 3 times under the same

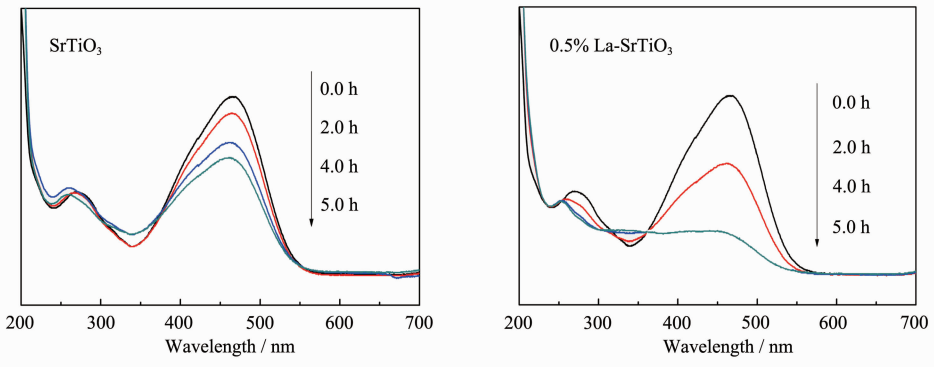

Fig.6　UV-Vis spectral of the MO aqueous solution under UV light irradiation in the presence of $SrTiO_3$ and 0.5% La-$SrTiO_3$ catalysts

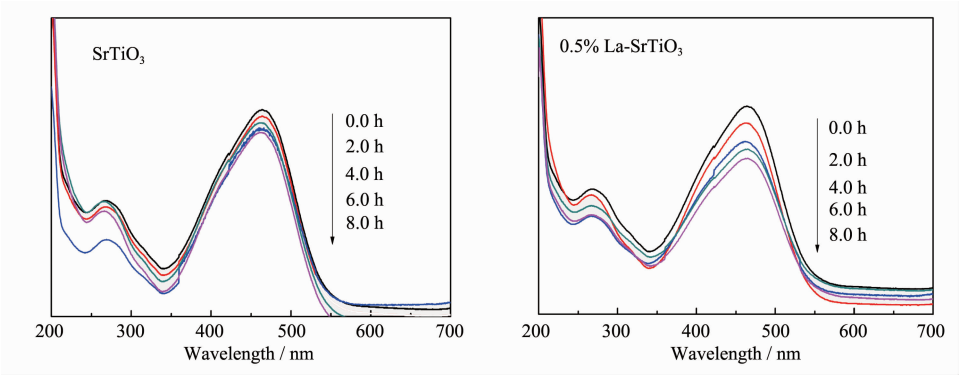

Fig.7 UV-Vis spectral of the MO aqueous solution under visible light irradiation in the presence of $SrTiO_3$ and 0.5% La-$SrTiO_3$ catalysts

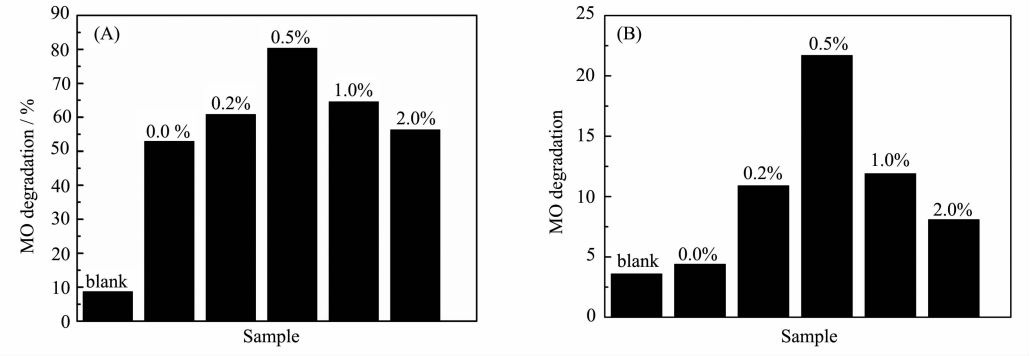

Fig.8 Photocatalytic activities of La-$SrTiO_3$ with different La content under UV (A) and visible (B) light irradiation for 2.0 h

conditions and the result is shown in Fig.9. The photocatalytic efficiency of the 0.5% La-$SrTiO_3$ catalyst decreases only 4.9% and 3.2% after three cycles under UV and visible light irradiation, respectively, which indicates that the catalyst is stable for the photocatalysis of MO molecules.

2.3 Adsorption of methyl orange

The photocatalysis performance has been significantly dependent on the adsorbability [10-11]. Therefore, a study of MO adsorption was performed on $SrTiO_3$ and 0.5% La-$SrTiO_3$ catalysts using 10 mg of catalyst at room temperature in the dark. The adsorption capacity of $SrTiO_3$ and 0.5% La-$SrTiO_3$ catalysts is displayed in Fig.10 (A), in which the adsorption behaviors of MO on $SrTiO_3$ and 0.5% La-$SrTiO_3$ catalysts follow the Langmuir model. It can be seen that MO uptake capacity strongly increases in the presence of the 0.5% La-$SrTiO_3$ catalyst compared to that of the $SrTiO_3$ catalyst. The adsorbed quantities of MO, q_t ($mg \cdot g^{-1}_{catalyst}$), at time t are calculated according to equation (**1**):

$$q_t = [(C_0 - C_t) \times 1000 \times M_W \times V_0]/w_{catalyst} \quad (1)$$

Where C_0 and C_t ($mol \cdot L^{-1}$) are the initial concentrations and concentration at time t of MO, respectively; M_W is the molecular weight of MO ($g \cdot mol$); V_0 is the volume of MO aqueous solution (L); and $w_{catalyst}$ is the mass of catalyst (g). The equilibrium adsorption capacity (q_e) and adsorption rate constant

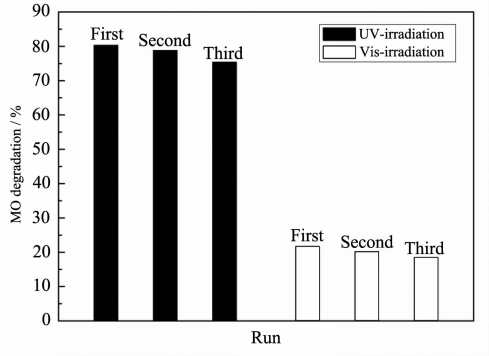

Fig.9 Cycling runs in photocatalytic degradation of MO in the presence of 0.5% La-$SrTiO_3$ catalyst under UV and visible light irradiation for 2.0 h

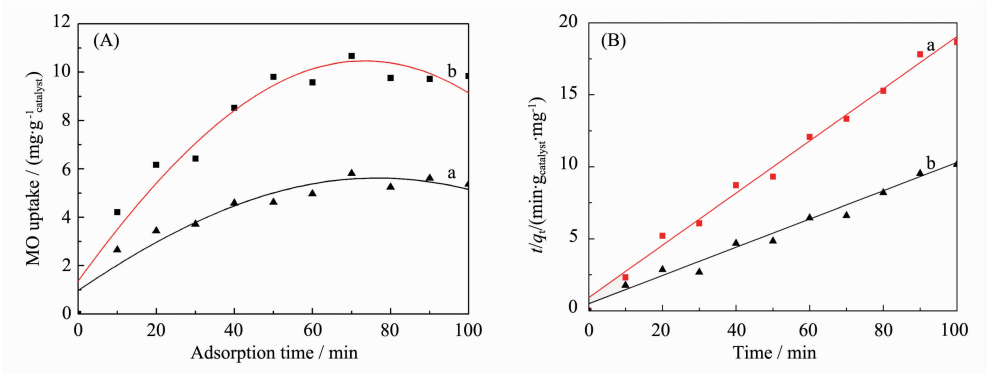

(a) $SrTiO_3$; (b) 0.5% La-$SrTiO_3$

Fig.10　MO adsorptivity (A) and second-order kinetic plots for the dye removal (B)

(k_{ads}) are usually estimated by the pseudo-first-order and pseudo-second-order model, and the correct values are chosen according to the higher correlation coefficient R^2 [12-13]. Here, the pseudo-second-order adsorption kinetics was adopted according to the adsorption equilibrium capacity in the form[13]:

$$t/q_t = [1/(k_{ads}q_e^2)]+t/q_e \quad (2)$$

Where q_e and q_t are the adsorption capacity at equilibrium and at time t, respectively (mg·$g^{-1}_{catalyst}$); and k_{ads} is the rate constant of the pseudo-second-order adsorption ($g_{catalyst}$·min^{-1}·mg^{-1}).

In this work, the experimental data evaluated from the linear transform $t/q_t=f(t)$ in Fig.10(B) exhibits the coincidence to the pseudo-second-order adsorption kinetics, therefore, the q_e and k_{ads} values are determined from the slope and intercept of the plot and shown in Table 2. It can be seen that the 0.5% La-$SrTiO_3$ catalyst shows better adsorptivity than that of the $SrTiO_3$ catalyst. The enhancement in adsorption performance of the 0.5% La-$SrTiO_3$ catalyst may be attributed to its higher BET specific surface area.

2.5　Light absorption

The UV-Vis diffuse reflectance spectra of $SrTiO_3$ and 0.5% La-$SrTiO_3$ samples are given in Fig.11. It can be seen that the 0.5% La-$SrTiO_3$ catalyst has much larger light absorption than pure $SrTiO_3$ sample

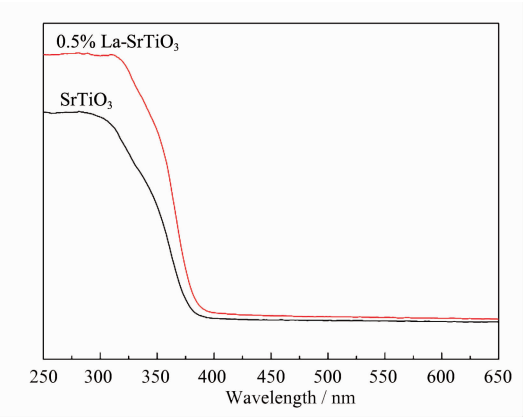

Fig.11　UV-Vis diffuse reflectance spectra of $SrTiO_3$ and 0.5% La-$SrTiO_3$ catalysts

in the wavelength ranging from 250 nm to 650 nm and the absorption edge of 0.5% La-$SrTiO_3$ sample is obviously red-shifted. The band-gap energy level of $SrTiO_3$ and 0.5% La-$SrTiO_3$ samples can be estimated from the intercept of UV-Vis diffuse reflectance spectra using the following equation: E_g=1 240/λ [14-15], and the results are listed in Table 2. As shown in Table 2, the values of band-gap energy level for 0.5% La-$SrTiO_3$ sample is lower than that of pure $SrTiO_3$ sample, revealing that the band-gap energy level is evidently decreased by doping the material with La. So the 0.5% La-$SrTiO_3$ sample shows a higher photocatalytic activity.

Table 2　Adsorption and band-gap energy level of $SrTiO_3$ and 0.5% La-SrO_3 catalysts

Catalyst	q_e / (mg·$g^{-1}_{catalyst}$)	k_{ads} / (g·mg^{-1}·min^{-1})	E_g / eV
$SrTiO_3$	5.09	0.040 63	3.22
0.5% La-SrO_3	10.32	0.018 78	3.18

3 Conclusions

In summary, La-doped $SrTiO_3$ catalysts with different La content have been synthesized by a sol-gel method. TEM and SEM results show that there is no big difference between $SrTiO_3$ and 0.5% La-$SrTiO_3$ samples in particle size and morphologies. With increasing La content, the photocatalytic activities of La-$SrTiO_3$ under UV and visible light irradiation first increase, reaching a maximum around La content of 0.5% and then decrease with further increasing La content. The 0.5% La-$SrTiO_3$ catalyst obviously exhibits much higher UV and visible light photoactivity than Pure $SrTiO_3$ catalyst and it is stable for the photocatalysis of methyl orange. The improved photocatalytic activities of 0.5% La-$SrTiO_3$ catalyst can be attributed to the increase of BET surface area, the enhancement in adsorption performance, the stronger absorption in 250 ~650 nm light region and the lower band-gap energy level.

Acknowledgments: We would like to thank the financial support from the National Science Foundations of China (No. 21171091) and the Natural Science Foundation of Higher Education Institutions in Anhui Province (KJ2012A217, KJ2012B136).

References:

[1] Jia A Z, Su Z Q, Lou L L, et al. *Solid State Sci*., **2010**,**12**: 1140-1145

[2] LI Rui-Pu(李瑞璞), LUO Wen-Jun(罗文俊), LI Zhao-Shen (李朝升), et al. *Chinese J. Inorg. Chem.* (*Wuji Huaxue Xuebao*), **2010**,**26**:149-152

[3] Sun Y, Liu J W, Li Z H. *J. Solid State Chem*., **2011**,**184**: 1924-1930

[4] Subramanian V, Roeder R K, Wolf E E. *Ind. Eng. Chem. Res*., **2006**,**45**:2187-2193

[5] Xie T H, Sun X Y, Lin J. *J. Phys. Chem. C*, **2008**,**112**:9753-9759

[6] Wang G Y, Qin Y, Cheng J, et al. *J. Fuel. Chem. Technol*., **2010**,**38**(4):502-507

[7] Wang D F, Ye J H, Kako T, et al. *J. Phys. Chem. B*, **2006**, **110**:15824-15830

[8] Ohno T, Tsubota T, Nakamura Y, et al. *Appl. Catal. A*: *General*, **2005**,**288**:74-79

[9] Li X, Ye J H. *J. Phys. Chem. C*, **2007**,**111**:13109-13116

[10]Chen X, Mao S S. *Chem. Rev*., **2007**,**107**:2891-2959

[11]Chen S F, Liu Y Z. *Chemosphere*, **2007**,**67**:1010-1017

[12]Kangwansupamonkon W, Jitbunpot W, Kiatkamjornwong S, et al. *Polym. Degrad. Stab*., **2010**,**95**(9):1894-1902

[13]Ho Y S, McKay G. *Trans. Inst. Chem. Eng*., **1998**,76B:332-340

[14]Sun H Q, Bai Y, Jin W Q. *Sol. Energy Mater. Sol. Cells*, **2008**,**92**:76-83

[15]Hagfeld A, Grätze M. *Chem. Rev*., **1995**,**95**:49-68